2024 IEEE 100th Vehicular Technology Conference (VTC2024-Fall) | 979-8-3315-1778-6/24/$31.00 ©2024 IEEE | DOI: 10.1109/VTC2024-Fall63153.2024.10757786

Power Allocation for Uplink Sensing and Communication in Cell-free ISAC Systems with Multi-Antenna Users and Multibeam

Igor B. Palhano★, Roberto P. Antonioli★, Yuri C. B. Silva★, Gábor Fodor†,‡, Walter C. Freitas★, Michel G. dos Santos★
Wireless Telecom Research Group (GTEL)★, Federal University of Ceará, Fortaleza, Brazil.
Ericsson Research† and Royal Institute of Technology‡, Stockholm, Sweden.
{igor.palhano, antonioli, yuri, walter, michel.gonzaga}@gtel.ufc.br, gabor.fodor@ericsson.com, gaborf@kth.se

***Abstract*—Driven by the expansion of enhanced mobile broadband and massive machine type communication use cases – including high-accuracy sensing services and radar sensing for autonomous vehicles – integrated sensing and communication using orthogonal frequency division multiplexing has been proposed for sixth generation systems. In this context, studying the possible system arrangements for cell-free networks is important to meet the upcoming requirements imposed on integrated sensing and communication systems. In this work, we evaluate the uplink communication of cell-free systems supporting integrated sensing and communications, i.e., when users transmit simultaneously sensing and communication signals while the access points act as receivers for both. To this end, multi-antenna users employ a multibeam solution for transmitting independent sensing and communication symbols, while adopting either singular value decomposition or angular beamforming. By means of Monte Carlo simulations, we show that the performance of the proposed multibeam solution yields high performance in terms of signal-to-interference-plus-noise ratio for both communication and sensing as well as a low spatial frequency error obtained via angular estimation using the multiple signal classification algorithm.**

***Index Terms*—Cell-free networks, integrated sensing and communication, multibeam, multiple signal classification (MUSIC), power allocation.**

I. Introduction

The current recommendations for International Mobile Telecommunications (IMT) for 2030 and beyond (IMT-2030), which includes the services expected for sixth generation (6G) networks, shows that, among the services that are already expected to evolve, it is expected that, with the increase in communication capacity and speed, sensing will be integrated into the communication network [1], [2].

In this sense, the evolution of the cell-free (CF) network architecture with cloud radio access network (C-RAN) is of interest for providing integrated sensing and communication (ISAC), since CF is already seen as a promising network architecture to be adopted in 6G networks in some deployment scenarios and has a high capacity for serving users with uniform service [3]. For the integration of sensing and communication as proposed in IMT-2030, the academic community has moved towards the study of radars based on the orthogonal frequency division multiplexing (OFDM) waveform, which is already used by cellular and wireless local area networks [4], although several multiple-input-multiple-output (MIMO) radar specialists are also investigating other possible waveforms to meet the expected ISAC requirements.

To integrate sensing into the communication network, there are basically two approaches when it comes to which entity transmits the sensing signals, namely, network (NW)-based or user equipment (UE)-based sensing. In the NW-based sensing, the sensing signals are transmitted by a base station (BS) or access point (AP), while the UE is responsible for transmitting the sensing signals in the UE-based sensing.

Existing works on cell-free systems supporting ISAC typically consider NW-based sensing, such as in [5]–[11]. Specifically, [5] proposes an optimized waveform and frame structure for communication and sensing, referred therein as joint communication and sensing (JCAS), where the BSs transmit the sensing signals in the downlink. In that study, the authors aim at achieving high communication rates and low interference via adaptive beamforming (BF). However, their proposed model is limited by the fact that it is based on obtaining the echoes of the signals used for channel estimation during the uplink (UL) period, thus making it unfeasible to implement in networks that use the OFDM waveform, which restricts the sensing echoes to the cyclic prefix.

In [6], the authors propose an ISAC model for downlink (DL) multi-static sensing, where they consider a scenario with perfect channel state information (CSI) and that the initial position of the target is known. That paper studiesa power optimization problem aimed at maximizing the target detection probability under signal-to-interference-plus-noise ratio (SINR) constraints for communication and a maximum transmit power available at the APs.

In [7], the authors propose a system for ISAC with a dedicated BS for communication, a dedicated BS for sensing, a UE, and a set of targets distributed around a specific angle with regard to the communication BS, which is previously known. That study compares single beam and multibeam schemes at the BS considering the DL of a bi-static scenario. Following a slightly different NW-based sensing approach, the authors in [11] consider a dedicated set of AP transmitting the sensing signal together with the UEs in the uplink, with the main goal of managing mutual interference using large processing gains, adaptive BF, spatial diversity and power allocation.

In this work, we consider a CF network with ISAC operating in the UL. Unlike the existing literature, we consider multi-antenna UEs transmitting both communication and

sensing symbols to the APs. To the best of our knowledge, this is the first work adopting such a UE-based sensing approach. Specifically, the UEs adopt a multibeam scheme [7], [8], where one beam is used for the communication symbols and a second beam is used for the sensing symbols. We assume that some a priori information about the area, where the targets are located, is available and, therefore, we allocate the APs closest to this region to act as sensing receivers. We design the beams used by the UEs using two classic methodologies: singular value decomposition (SVD) BF [12] and angular BF [13]. In the simulations, we consider different power allocations among the beams used for sensing and communication, and show that the proposed multibeam solution yields high performance in terms of SINR for both communication and sensing as well as a low spatial frequency error obtained via angular estimation from the multiple signal classification (MUSIC) algorithm.

II. System Model

A. Cell-free Network Supporting ISAC

We consider a CF ISAC system with a C-RAN architecture following a UL sensing framework. Here, M APs equipped with N_{rx} antennas and connected to a single central processing unit (CPU) are serving K UEs, each equipped with N_{tx} antennas. Furthermore, there are L targets distributed in the network. We also consider a UL operation in time division duplex (TDD) fashion and adopt a block fading model, as in [3]. The adopted frame structure is illustrated in Figure 1.

In the considered UL phase with duration of τ_u symbols, all UEs transmit both unknown communication symbols and already known sensing symbols (i.e., pilots for sensing) [9], thus each UE acts as communication transmitter (Tx-c) and sensing transmitter (Tx-s). The UEs use a multibeam scheme for transmitting communication and sensing symbols, as will be explained in Section III. Also, in the UL period, we assume that there are two groups of APs: one group for communication reception and a second group for sensing reception (i.e., the sensing receivers), exemplified in Figure 2. Thus, each AP either acts as communication receiver (Rx-c) or sensing receiver (Rx-s). In this work we consider perfect CSI, which is assumed to be known at the CPU and UEs [7], [9], [10].

In this work, we assume that there is a previous processing in the network that finds a possible area where the target might

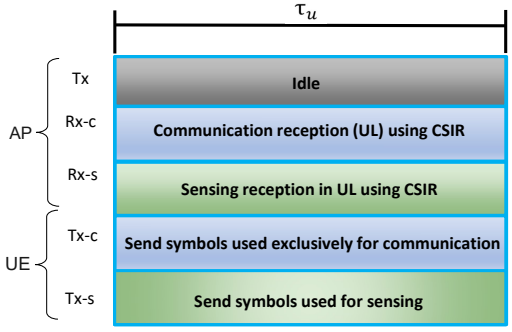

Fig. 1: Frame structure for uplink ISAC. Note that the UE acts as a Tx node for sensing and communication (Tx-s and Tx-c), while the AP acts as an Rx node for both (Rx-s and Rx-c).

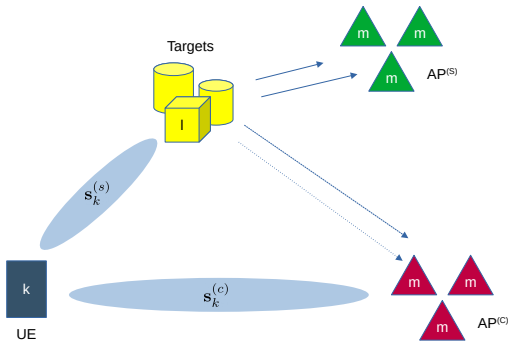

Fig. 2: Adopted multibeam approach with UE transmitting independent beams for sensing and communication.

be, i.e., unlike what is assumed in [10], we do not assume that the target position is known, but rather that we know a region where the possibility of the target existence is higher than in the rest of the network. From this, the CPU will take the minimum number of APs that are closest to the l-th target, making a cluster of APs dedicated to sensing symbols, as exemplified in Figure 3.

Note that the orange dots in the figure will be the nearest APs to the l-th target (the red dot). Since we can cluster APs for sensing and the position of AP is known at the CPU, we can determine a coordinate for the center of the cluster.

B. Signal Model

Let $\mathbf{y}_m \in \mathbb{C}^{N_{\text{rx}}}$ be the received signal at the m-th AP

$$\mathbf{y}_m = \sum_{k=1}^{K} \sqrt{\rho_k^{(c)}} \mathbf{H}_{k,m}^{(c)} \mathbf{w}_k^{(c)} s_k^{(c)} + \sum_{k=1}^{K} \sqrt{\rho_k^{(s)}} \mathbf{H}_{k,m}^{(s)} \mathbf{w}_k^{(s)} s_k^{(s)} + \mathbf{n}_m, \tag{1}$$

where $\rho_k^{(c)}$ and $\rho_k^{(s)}$ represent the k-th UE transmission power for communication and sensing symbols, respectively, $\mathbf{H}_{k,m}^{(c)} \in \mathbb{C}^{N_{\text{rx}} \times N_{\text{tx}}}$ and $\mathbf{H}_{k,m}^{(s)} \in \mathbb{C}^{N_{\text{rx}} \times N_{\text{tx}}}$ represent the communication and sensing channel between the k-th UE and m-th AP, respectively. The vectors $\mathbf{w}_k^{(c)} \in \mathbb{C}^{N_{\text{tx}}}$ and $\mathbf{w}_k^{(s)} \in \mathbb{C}^{N_{\text{tx}}}$ represent the beamformer of the k-th UE for communication and sensing, respectively. Finally, $\mathbf{n}_m \in \mathbb{C}^{N_{\text{rx}}}$ represents the additive white Gaussian noise (AWGN) at the m-th AP, which is modeled as $\mathbf{n}_m \sim \mathcal{CN}(0, \mathbf{I}_{N_{\text{rx}}} \sigma_n^2)$, where σ_n is the standard deviation of noise, modeled as $\sigma_n = Bk_B T_0 \sigma_f$, where B

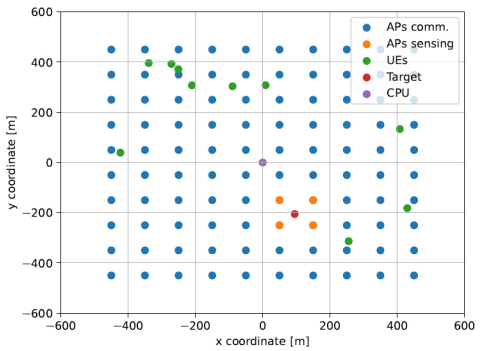

Fig. 3: Example of the adopted cell-free scenario with the cluster of sensing APs surrounding the target.

is the bandwidth, k_B is the Boltzmann's constant, T_0 is the temperature and σ_f is the noise figure.

The chosen channel model is based on [8]. Let P represent the number of multi-paths in the channel, in this way

$$\mathbf{H}_{k,m}^{(c)} = \sum_{p=1}^{P} \beta_{k,m} \mathbf{a}(\theta_{m,p}, \phi_{m,p}) \mathbf{a}^H(\theta_{k,p}, \phi_{k,p}), \tag{2}$$

where $\beta_{k,m} \in \mathbb{C}$ is the large scale fading factor between the k-th UE and m-th AP, $\mathbf{a}(\theta_{m,p}, \phi_{m,p})$ and $\mathbf{a}(\theta_{k,p}, \phi_{k,p})$ represent the steering vectors relative to the p-th path constructed by the angle of arrival (AoA) at the m-th AP and angle of departure (AoD) at the k-th UE, respectively, with θ representing the azimuth angle and ϕ representing the elevation angle. The generic steering vector relative to indexes a and b is given by

$$\mathbf{a}(\theta_{a,b}, \phi_{a,b}) = \frac{1}{\sqrt{N_{\text{rx}}}} [1, e^{-j\pi \sin(\phi_{a,b}) \cos(\theta_{a,b})}, \ldots, e^{-j\pi (N_{\text{rx}}) \sin(\phi_{a,b}) \cos(\theta_{a,b})}]. \tag{3}$$

For the sensing channel, assuming L targets, the steering vectors that compose $\mathbf{H}_{k,m}^{(s)}$ will be generated by the sum of AoDs from UEs to targets, and AoAs from targets to APs

$$\mathbf{H}_{k,m}^{(s)} = \sum_{l=1}^{L} \alpha_l \beta_{k,m} \mathbf{a}(\theta_{m,l} \phi_{m,l}) \mathbf{a}^H(\theta_{k,l}, \phi_{k,l}), \tag{4}$$

where α_l is the radar cross section (RCS) value of the l-th target. Furthermore, the combining vector $\boldsymbol{\nu}_k^{(u)} \in \mathbb{C}^{M N_{\text{rx}} \times 1}$ at the CPU, assuming joint receive processing, relative to transmit symbol u of the k-th UE, is modeled as in [3, Chapter 01], from the effective channel of the k-th UE $\mathbf{H}_k^{(u)}$, which is obtained by vertically stacking the channel matrices relative to each AP for a given UE k, i.e., $\mathbf{H}_k^{(c)} \in \mathbb{C}^{M N_{\text{rx}} \times N_{\text{tx}}}$ and $\mathbf{H}_k^{(s)} \in \mathbb{C}^{M^{(s)} N_{\text{rx}} \times N_{\text{tx}}}$ for communication and sensing, where $M^{(s)}$ denotes the number of sensing cluster APs. Following the proposed model, the SINR $\Gamma_k^{(u)}$ for each symbol u transmitted by the k-th UE will be

$$\Gamma_k^{(u)} = \frac{|(\boldsymbol{\nu}_k^{(u)})^H \mathbf{H}_k^{(u)} \mathbf{w}_k^{(u)}|^2 \rho_k^{(u)}}{I_k^{(u)} + \sigma_n^2}, \tag{5}$$

where the interference term $I_k^{(u)}$ is given by

$$I_k^{(u)} = \sum_{j=1}^{K} \sum_{i \in \{c,s\}} |(\boldsymbol{\nu}_k^{(u)})^H \mathbf{H}_j^{(i)} \mathbf{w}_j^{(i)}|^2 \rho_j^{(i)} - |(\boldsymbol{\nu}_k^{(u)})^H \mathbf{H}_k^{(u)} \mathbf{w}_k^{(u)}|^2 \rho_k^{(u)}. \tag{6}$$

C. Sensing Metric

In this work, in order to avoid possible ambiguity problems generated by the dominance of the angles used in (3), we adopt as sensing metric the mean square error (MSE) of the product of the spatial frequency of the angles estimated via the MUSIC algorithm, that is,

$$\text{MSE} = \frac{1}{M^{(s)} L} \sum_{m=1}^{M^{(s)}} \sum_{l=1}^{L} (\sin(\hat{\phi}_{m,l}) \cos(\hat{\theta}_{m,l}) - \sin(\phi_{m,l}) \cos(\theta_{m,l}))^2, \tag{7}$$

where $\sin(\phi_{m,l}) \cos(\theta_{m,l})$ represents the normalized spatial frequency [14] generated from the l-th target and m-th sensing AP, while $\sin(\hat{\phi}_{m,l}) \cos(\hat{\theta}_{m,l})$ denotes the estimated normalized spatial frequency reconstructed using the estimated elevation angle $\hat{\phi}_{m,l}$ and the estimated azimuth angle $\hat{\theta}_{m,l}$, both obtained via MUSIC algorithm.

It is important to note that, due to the multiplicative structure of the MSE metric adopted in this work, we will have a possible multi-modal curve, with the modes being the elevation and azimuth error averages.

III. Beamforming techniques

In this work, we study two different BF techniques, namely SVD BF [12] and angular BF [13]. We assume that all radio frequency (RF) chains are connected and used for the proposed digital BF, as exposed in [15]. Furthermore, we will only consider the strongest line-of-sight component of the communication channel, i.e., assuming $P = 1$.

A. SVD Beamforming

Let us apply the SVD decomposition to the effective channel matrix $\mathbf{H}_k^{(u)}$, relative to communication or sensing, to generate the corresponding BF vector, which is expressed as

$$\mathbf{H}_k^{(u)} = \mathbf{U}_k \boldsymbol{\Sigma}_k \mathbf{V}_k^H. \tag{8}$$

The columns of $\mathbf{U}_k$ represent the left singular vectors, and $\boldsymbol{\Sigma}_k$ represents the singular value diagonal matrix, and the columns of $\mathbf{V}_k$ represent the right singular vectors. The first column of $\mathbf{V}_k$, denoted by $\mathbf{v}_k \in \mathbb{C}^{N_{\text{tx}}}$, is the vector that maximizes $\|\mathbf{H}_k^{(u)} \mathbf{v}_k\|_2$ [16], and expresses the direction of the greatest gain for symbol u of the k-th UE. Hence, BF is set as $\mathbf{w}_k^{(u)} = \mathbf{v}_k$. The same process is applied to both $\mathbf{H}^{(s)}$ and $\mathbf{H}^{(c)}$.

B. Angular Beamforming

Let $\boldsymbol{\beta}_k \in \mathbb{C}^M$ represent a vector containing the large-scale fading coefficients between the k-th UE and all APs. Assuming that this information is known at the CPU, then it is possible to find the AP m^* with the highest coefficient as

$$m^* = \arg \max_m \boldsymbol{\beta}_k, \tag{9}$$

and reconstruct the steering vector using the AoD between the i-th UE and the m^*-th AP. Hence, for communication BF we will have

$$\mathbf{w}_k^{(c)} = \mathbf{a}(\theta_{k,m^*}, \phi_{k,m^*}) \in \mathbb{C}^{N_{\text{tx}}}. \tag{10}$$

For sensing BF we will generate a steering vector to the center of the sensing APs, as exemplified in Figure 3. Let us denote this center as $m^{(s)}$. The sensing BF vector is then given by

$$\mathbf{w}_k^{(s)} = \mathbf{a}(\theta_{k,m^{(s)}}, \phi_{k,m^{(s)}}) \in \mathbb{C}^{N_{\text{tx}}}, \tag{11}$$

which guarantees that sensing symbols are pointed to a region that maximizes the l-th target impact on received signals.

IV. Numerical Results

In order to assess the impact of UE-based sensing on the UL communication performance, we perform snapshot-based link level simulations and compute both the SINR and the spatial frequency MSE. The latter is obtained via MUSIC algorithm to estimate both azimuth and elevation angles.

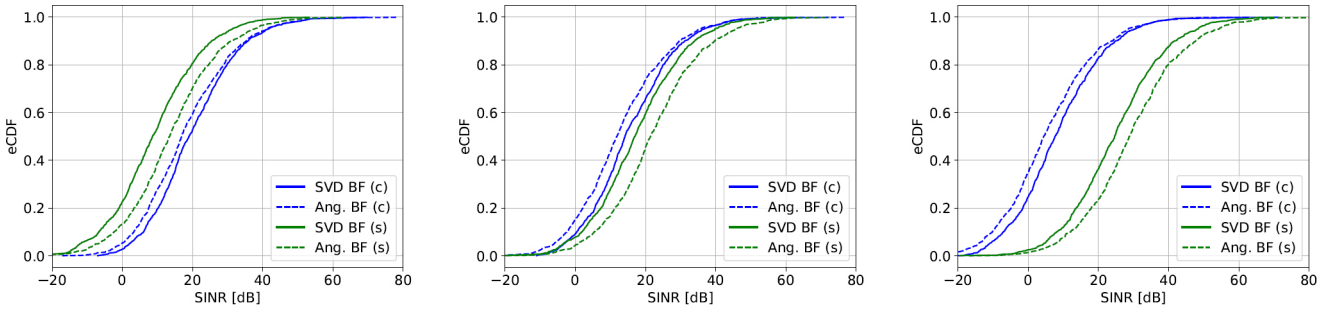

(a) 90%-comm./10%-sensing. **(b)** 50%-comm./50%-sensing. **(c)** 10%-comm./90%-sensing.

Fig. 4: SINRs for communication and sensing with SVD and angular beamforming and varying beam power allocation.

A. Scenario Description

The considered simulation scenario contains $M = 100$ APs with $N_{\text{rx}} = 8$ antennas each, $K = 10$ UEs with $N_{\text{tx}} = 4$ antennas each and $L = 1$ target. The APs are positioned in a grid architecture, as exemplified in Figure 3, while the UEs and targets positions are randomly distributed in a grid with 500×500 m^2 of area. The carrier frequency, bandwidth, noise figure, and temperature are set to 1.9 GHz, 20 MHz, 9 dB, and 298 K, respectively. Furthermore, the APs height is 11.5 m, the UEs height is 1.5 m and the targets height is 0m. The total transmission power of the UEs is 24 dBm and the proportion of the power allocated from the communication beam to the sensing beam is fixed for each of the simulated scenarios. In the first scenario, the transmission power for communication is 90% of the total power of the UEs (i.e., the sensing power is 10% of the total power), referred to as 90%-comm./10%-sensing. The second scenario consider an equal distribution of power for communication and sensing (i.e. 50% for communication and 50% for sensing), referred to as 50%-comm./50%-sensing, and finally, the system's behavior is checked when 10% of the UE's power is allocated to communication and the rest to sensing, referred to as 10%-comm./90%-sensing.

The large scale fading coefficients $\beta_{k,m}$ between the k-th UE and m-th AP are generated using a three slope path-loss model, and the shadowing standard deviation $\sigma_s = 8$ dB. The large-scale fading is calculated as in [17].

The l-th target RCS is modeled by the Swerling-I model, where $\alpha_l \sim \mathcal{CN}(0, \sigma^2_{RCS})$, as in [10]. The azimuth and elevation angles are calculated by the generated positions of network elements. The results here presented were obtained considering 1000 Monte Carlo realizations.

B. Results and Discussion

In Figure 4 we have the empirical cumulative distribution function (eCDF) of the SINR in dB of the two proposed algorithms for the communication and sensing processing, also considering the three different power allocation scenarios. Initially, in Figure 4a, we can see that the SINR curves have a difference between the two BFs methodologies. At the 20-th percentile, the SINRs detection has a difference of 4.2 dB with the Angular BFs solution being the best, while at the same percentile, the communication SINRs have a difference of 2.65 dB with the SVDs solution now being the best.

It is known that beam pointing via SVD tends to be more effective when a large number of receiver antennas is available, as is the case with the proposed network, while angular pointing tends to be less effective, because it is based on pointing only in the direction of greatest gain, which does not necessarily reflect the best propagation space for communication.

Concerning the results obtained for sensing SINR, we can see that for the sensing scenario, the angular BF is more efficient than the BF based on SVD. This effect is due to the density of the adopted CF network, where, on average, each AP covers a small area of the network. Therefore, by pointing at $m^{(s)}$, the APs point approximately at the target, maximizing the signal strength of the signal redirected to the sensing APs.

In Figure 4b, we can see that the SINR using BF based on SVD for communication and sensing has a difference in the 20-th percentile of only 1.7 dB, while in the same percentile we observe a difference of 9.14 dB between the curves of SINR with angular BF. This large difference can be explained by a lower proportion of power for communication, since for angular BF to be effective for communication, we need a high amount of power to compensate for the loss generated by pointing, since the direction with the highest gain is not necessarily the one with the highest spectral efficiency.

In Figure 4c, due to the low proportion of power for communication, we observe that the 20-th percentile of the communication SINR does not reach 0 dB, while the sensing SINR is around 17 dB higher than that for communication, for a reason similar to the behavior of the previous curve.

Figure 5 shows the eCDF of the normalized spatial frequency MSE in dB for the two proposed BF algorithms. In Figure 5a, whose power proportions are 90% for communication and 10% for sensing, we found errors on the scale of -1.11 dB for SVD BF and -2.59 dB at the 80-th percentile for angular BF. This behavior can be justified by the type of pointing we expect from each technique. Revisiting the SINR graphs, note that BF based on SVD has good efficiency when directing the beams, proving to be a good option regarding angular formatting in this type of scenario. Observing Figure 5b, it is clear that angular BF has a lower MSE than the technique based on SVD, where angular BF

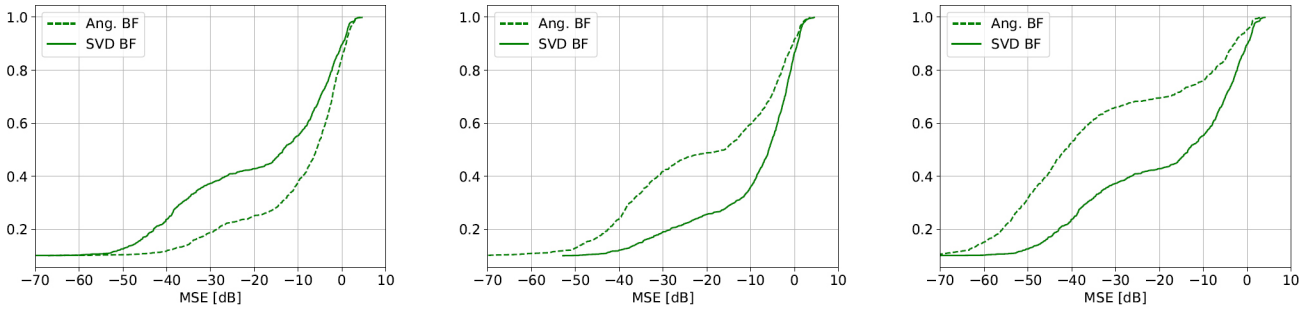

(a) 90%-comm./10%-sensing. **(b)** 50%-comm./50%-sensing. **(c)** 10%-comm./90%-sensing.

Fig. 5: $10\log_{10}(\text{MSE})$ of spatial frequency with SVD and angular beamforming and varying beam power allocation.

reaches an MSE of −2.9 dB while SVD BF achieves −0.84 dB at the same percentile. In Figure 5c, notice that in the 80-th percentile the error reached by the scenario with angular BF is approximately −7 dB, while the error with SVD BF is approximately −2 dB. Due to the low variability of the elevation angle caused by the chosen simulation parameters, we can see in Figure 5 that all curves have a multi-modal eCDF pattern, a behavior caused by the difference in the averages of the elevation and azimuth angle estimation error distributions, so we can see a saturation zone in the region between −40 and −20 dB.

V. Conclusion

The proposed UE-based sensing approach for ISAC in CF scenarios can perform communication with satisfactory quality of service and is capable of collecting signals related to data processing and sensing with sufficient quality to guarantee the estimation of parameters such as position, speed and RCS.

For future work, it would be relevant to analyze techniques for directing users' beams that guarantee the high performance shown here and balances the weights of these beams based on their transmission powers. Ideal power proportion would ensure high quality of communication and sensing. Finally, an analysis of the robustness of the system and the techniques in this work would allow to verify the behavior of the quality metrics of the system under realistic conditions, including imperfect CSI.

VI. Acknowledgment

This work was supported in part by Ericsson Research, Sweden, and Ericsson Innovation Center, Brazil, Technical Cooperation Contract UFC.50, in part by the Brazilian National Council for Scientific and Technological Development (CNPq), in part by FUNCAP, in part by FUNCAP/Universal Grant UNI-0210-00043.01.00/23, in part by CAPES - Finance Code 001, in part by CAPES/PRINT Grant 88887.311965/2018-00, and in part by CNPq/INCT-Signals Grant 406517/2022-3. G. Fodor was supported by the EU Horizon Europe Program, Grant No: 101139176 6G-MUSICAL.

References

[1] ITU, "Framework and overall objectives of the future development of IMT for 2030 and beyond," Recommendation ITU-R M.2160-0, Nov. 2023.

[2] A. Guidotti, A. V. Coralli, M. E. Jaafari, N. Chuberre *et al.*, "Role and evolution of non-terrestrial networks toward 6G systems," *IEEE Access*, vol. 12, pp. 55 945–55 963, 2024.

[3] Ö. T. Demir, E. Björnson, L. Sanguinetti *et al.*, "Foundations of user-centric cell-free massive MIMO," *Foundations and Trends® in Signal Processing*, vol. 14, no. 3-4, pp. 162–472, 2021.

[4] A. Chowdhury and C. R. Murthy, "How resilient are cell-free massive MIMO OFDM systems to propagation delays?" in *Proc. of IEEE SPAWC*, 2023, pp. 581–585.

[5] F. Liu, C. Masouros, A. Petropulu, H. Griffiths, and L. Hanzo, "Joint radar and communication design: Applications, state-of-the-art, and the road ahead," *IEEE Trans. on Commun.*, vol. 68, no. 6, pp. 3834–3862, 2020.

[6] Z. Behdad, O. T. Demir, K. W. Sung, E. Björnson, and C. Cavdar, "Multi-static target detection and power allocation for integrated sensing and communication in cell-free massive MIMO," *IEEE Trans. on Wireless Commun.*, pp. 1–1, 2024.

[7] M. U. Baig, J. Vinogradova, G. Fodor, and C. Mollen, "Joint communication and sensing beamforming for passive object localization," in *Proc. of WSA & SCC*, 2023, pp. 1–6.

[8] J. A. Zhang, X. Huang, Y. J. Guo, J. Yuan, and R. W. Heath, "Multibeam for joint communication and radar sensing using steerable analog antenna arrays," *IEEE Trans. on Veh. Technol.*, vol. 68, no. 1, pp. 671–685, 2019.

[9] S. Lu, F. Liu, F. Dong, Y. Xiong, J. Xu, and Y.-F. Liu, "Sensing with random signals," in *IEEE ICASSP*, 2024, pp. 12 961–12 965.

[10] Z. Behdad, Ö. T. Demir, K. W. Sung, E. Björnson, and C. Cavdar, "Power allocation for joint communication and sensing in cell-free massive MIMO," in *Proc. of IEEE GLOBECOM*, 2022, pp. 4081–4086.

[11] A. Sakhnini, A. Bourdoux, and S. Pollin, "A distributed radar and communication system with interference cancellation and power control," Mar. 2024. [Online]. Available: http://dx.doi.org/10.36227/techrxiv.171169321.12466725/v1

[12] G. M. Zilli and W.-P. Zhu, "Constrained-SVD based hybrid beamforming design for millimeter-wave communications," in *Proc. of IEEE VTC-Fall*, 2020, pp. 1–5.

[13] A. Innok, P. Uthansakul, and M. Uthansakul, "Angular beamforming technique for MIMO beamforming system," in *2012 9th International Conference on Electrical Engineering/Electronics, Computer, Telecommunications and Information Technology*, 2012, pp. 1–4.

[14] H.-L. Chiang, T. Kadur, and G. Fettweis, "Analyses of orthogonal and non-orthogonal steering vectors at millimeter wave systems," in *2016 IEEE 17th International Symposium on A World of Wireless, Mobile and Multimedia Networks (WoWMoM)*, 2016, pp. 1–6.

[15] J. Zhang, X. Yu, and K. Letaief, "Hybrid beamforming for 5G and beyond millimeter-wave systems: A holistic view," *IEEE Open Journal of the Commun. Society*, vol. 1, pp. 77–91, 01 2020.

[16] H. Golub, Gene and F. Van Loan, Charles, *Matrix Computation 4*. Johns Hopkins University Press, 2012.

[17] I. M. Braga, R. P. Antonioli, G. Fodor, Y. C. B. Silva, and W. C. Freitas, "Decentralized joint pilot and data power control based on deep reinforcement learning for the uplink of cell-free systems," *IEEE Trans. on Veh. Technol.*, vol. 72, no. 1, pp. 957–972, 2023.